

Article

Mechanical Properties of the Ti_{49.8}Ni_{50.2} Alloy after Multi-Axial Forging at 573 K

Aleksandr Lotkov ^{*}, Oleg Kashin, Victor Grishkov, Dorzhima Zhapova, Konstantin Krukovskii, Angelina Gusarenko , Natalia Girsova, Dmitrii Bobrov and Olga Kashina

Institute of Strength Physics and Materials Science, Siberian Branch of the Russian Academy of Science, 634055 Tomsk, Russia; okashin@ispms.ru (O.K.); grishv@ispms.ru (V.G.); dorzh@ispms.tsc.ru (D.Z.); kvk@ispms.tsc.ru (K.K.); aag@ispms.ru (A.G.); girsova@ispms.tsc.ru (N.G.); chromium76@gmail.com (D.B.); ocash@ispms.ru (O.K.)

* Correspondence: lotkov@ispms.tsc.ru; Tel.: +7-382-249-26-96

Abstract: The mechanical properties of Ti_{49.8}Ni_{50.2} (at %) alloy under tension at room temperature are studied in dependence on the true strain ($\epsilon = 1.84\text{--}9.55$) specified during isothermal multi-axial forging (abc-pressing). It was found that the stress at the beginning of the pseudoyield plateau does not depend on the value of the true abc-strain. It was found that after abc-pressing, already at a true strain $\epsilon = 1.84$, the yield stress σ_y was 900 ± 25 MPa, which is more than twice as high as compared to σ_y in the initial state of the specimens. With a further increase in the abc-strain, the yield stress continues to increase slightly and reaches 1000 ± 25 MPa at $\epsilon = 9.55$. In this case, the ultimate tensile strength of the samples increases by about 15%. The strain-hardening coefficient $\theta = d\sigma/d\epsilon$ at the III (linear) stage of the $\sigma(\epsilon)$ curve has a similar dependence on ϵ . It is shown that after abc-pressing with ϵ from 1.84 to 9.55, the yield stress and ultimate tensile increase linearly with increasing $d^{-1/2}$ in accordance with the Hall–Petch relation, where d is the average grain–subgrain size.

Keywords: titanium nickelide; isothermal multi-axial forging; mechanical properties; submicrocrystalline structure; Hall–Petch relation



Citation: Lotkov, A.; Kashin, O.; Grishkov, V.; Zhapova, D.; Krukovskii, K.; Gusarenko, A.; Girsova, N.; Bobrov, D.; Kashina, O. Mechanical Properties of the Ti_{49.8}Ni_{50.2} Alloy after Multi-Axial Forging at 573 K. *Metals* **2022**, *12*, 1043. <https://doi.org/10.3390/met12061043>

Academic Editors: Shi-Hoon Choi and Atef Saad Hamada

Received: 27 April 2022

Accepted: 16 June 2022

Published: 18 June 2022

Publisher's Note: MDPI stays neutral with regard to jurisdictional claims in published maps and institutional affiliations.



Copyright: © 2022 by the authors. Licensee MDPI, Basel, Switzerland. This article is an open access article distributed under the terms and conditions of the Creative Commons Attribution (CC BY) license (<https://creativecommons.org/licenses/by/4.0/>).

1. Introduction

The unique properties of titanium nickelide, such as the shape memory effect and pseudoelasticity, ensured its wide application in engineering and medicine. Titanium nickelide has high corrosion resistance and good strength properties with high ductility. Nevertheless, when titanium nickelide is used in load-bearing structures, increasing its strength characteristics is an urgent task. In particular, for the efficient use of TiNi-based alloys and their functional properties (shape memory effect and superelasticity), it is required to increase their yield stress and ultimate tensile strength while maintaining the plasticity of these materials. One of the ways to increase the yield stress and ultimate tensile strength of polycrystalline metals and alloys is the refinement of the grain structure by the methods of severe plastic deformation (SPD) [1,2]. To date, a number of models of microstructure transformation during SPD have been developed for various metals and alloys, a summary of which is presented in reviews [3–5]. Basically, these models are based on experimental data obtained on metals and alloys with different structures. The available experimental data show that both the material parameters (initial average grain size, phase composition, internal substructure, stacking fault energy) and the parameters of the SPD process (method SPD, strain value, strain rate, temperature, strain path) have influence on the refinement of grain–subgrain structure and corresponding changes of the functional and deformation characteristics of materials. Therefore, it is important to obtain experimental regularities in the formation of the microstructure and physical and mechanical properties of TiNi-based alloys, which are obtained using a specific SPD method.

In most works devoted to the study of the regularities of grain structure refinement during SPD and the corresponding changes in the properties of metals and alloys, including TiNi-based alloys, SPD methods such as equal channel angular pressing, high-pressure torsion, cold rolling, and twist extrusion, often in combination with thermomechanical treatments, were used [3–5]. In particular, after isothermal equal-channel angular pressing at 573–723 K in binary TiNi-based alloys on TiNi with 49.7, 50.2, 50.6 at % Ni, submicrocrystalline structures with an average grain–subgrain size from 0.1 to 0.23 μm were obtained [6–8]. This caused an increase in the yield stress, σ_y , and ultimate tensile strength, σ_{UTS} , by 2.3 and 1.5 times, respectively. One of the well-known methods of severe plastic deformation, which makes it possible to obtain an ultrafine-grained structure in metals and alloys, is the forging method with a change in the deformation axis in three mutually orthogonal directions, which is called “multi-axial forging” or “abc-pressing” [9–14]. The abbreviation “abc-pressing” was used in further text. This method was used in [10–12] for processing a binary TiNi-based alloy near the equiatomic composition. In these works, experimental data were obtained on the evolution of the microstructure and properties of this alloy as a result of abc-pressing at different conditions. In [10,11], abc-pressing of the $\text{Ti}_{49.8}\text{Ni}_{50.2}$ alloy was carried out with a stepwise decrease in the deformation temperature in the sequence: 873 K–673 K–623 K–573 K. The specified true deformation reached ≈ 2 at each pressing temperature. After final pressing at 573 K, a microstructure with grain–subgrain sizes from 20 to 300 nm was obtained. In this case, σ_{UTS} increases by a factor of 1.6 relatively to σ_{UTS} in the original coarse-grained samples. It was shown in [12] that isothermal abc-pressing of the $\text{Ti}_{49.9}\text{Ni}_{50.1}$ alloy at 423 K and 673 K leads to a strong refinement of the grain structure of the samples. However, a detailed analysis of the average sizes of grains–subgrains was not carried out in [12]. It was only shown that after pressing at 423 K, there are nanograins with a size of ≈ 20 nm, but their volume fraction was not estimated. The ultimate tensile strength of the $\text{Ti}_{49.9}\text{Ni}_{50.1}$ alloy after pressing at 673 K and 423 K increases by factors of 1.5 and 1.9, respectively, as compared with the σ_{UTS} of the original coarse-grained specimens. However, these data are insufficient to reveal the relationship between the resulting microstructure and mechanical properties. For this, studies are needed with a wider variation in the parameters of the abc-pressing process. In particular, an important SPD parameter is the deformation temperature [1–8]. It was shown in [13] that after abc-pressing at 723 K, the coarse-grained (40 μm) structure of the $\text{Ti}_{49.8}\text{Ni}_{50.2}$ alloy transforms into a structure with an average grain size of 1 μm as the true deformation increases to 8.44. Such a refinement of the grain structure had practically no effect on the ultimate tensile strength, but the yield strength increased by ≈ 2 times. In [14], the evolution of the microstructure of a nickel–titanium binary alloy with a nickel content of 50.2 at % after abc-pressing at a temperature of 573 K was studied. It was shown that with an increase in the total true strain during abc-pressing, the grain–subgrain structure is refined to an ultrafine-grained state: the grain–subgrain size was 130 nm at the maximum studied abc-strain $\epsilon = 9.55$. It might be expected that more substantial grain refinement after abc-pressing at 573 K can provide the more large increment in mechanical properties of this alloy. The aim of this work is to study the effect of microstructure transformation as a result of abc-pressing at 573 K on the mechanical properties of the $\text{Ti}_{49.8}\text{Ni}_{50.2}$ (at %) alloy.

2. Materials and Methods

The studies were performed on the $\text{Ti}_{49.8}\text{Ni}_{50.2}$ (at %) alloy produced by MATEK-SMA Ltd. (Moscow, Russia). This choice is due to the fact that this alloy belongs to non-aging alloys, which excludes the formation of the Ti_3Ni_4 secondary phase during SPD.

As the initial state, the state of the alloy was chosen after the formation of a workpiece in the form of a cube with a side of 20 mm, which was obtained by one cycle of abc-pressing at a temperature of 1073 K. The initial samples were placed in a mold and kept in a furnace at a temperature of 573 K for 10 min, after which the mold with the sample was placed on a hydraulic press and the sample was compressed at a rate of 0.16–0.18 s^{-1} . The temperature decreases of the samples at the end of each compression act did not exceed 10 K. Each cycle

of abc-pressing includes the sample compression in three mutually perpendicular directions. After each act of compression, the sample was removed from the mold and, without cooling, was again placed in the mold in such a way as to ensure that the sample was deformed in a perpendicular direction relative to the direction of the previous deformation. In each cycle of abc-pressing, the total specified true strain reached 0.95 ± 0.10 . To set the planned strain of the sample, the cycle of its three compressions was repeated several times. Samples were obtained with a true strains of 1.84; 3.60; 5.40; 7.43; and 9.55.

The microstructure of the alloy was studied by light optical microscopy (Zeiss Axiovert-200M, (Carl Zeiss AG, Oberkochen, Germany)), scanning (Zeiss LEO EVO 50 XVP (Carl Zeiss AG, Oberkochen, Germany)) and transmission electron microscopy JEM-2100 (JEOL Ltd., Tokyo, Japan). Samples for microstructure examination were cut using an electric discharge machine. After cutting, the surfaces of the specimens were mechanically polished using a Saphir 350 grinder (Audit Diagnostics, Bussiness & Technology Park, Carrigtwohill. Co. Cork, Ireland) and abrasive paper (silicon carbide with a gradual decrease in grain size to 1200). Finally, the surfaces of the samples were finished with diamond paste with a dispersion of 3 μm .

The study of the microstructure by transmission electron microscopy (TEM) was carried out using thin foils. Thin plates 0.4 mm thick were cut from blanks obtained after abc-pressing using an electric discharge machine. The final foil was obtained either by electrolytic polishing in an electrolyte containing sulfuric, nitric and hydrofluoric acids in a ratio of 6:1:3 or by ion etching on an Ion-slicer EM-09 100 15 devices (JEOL Ltd., Tokyo, Japan).

X-ray diffraction analysis of the samples was carried out using a DRON-7 X-ray diffractometer with $\text{Co-K}\alpha$ radiation (JSC IC Bourestvic, St. Petersburg, Russia). The diffraction patterns of the samples with the structure of the cubic B2 phase were obtained at 393 K. The Williamson–Hall full-profile analysis [15,16] was used to separate the contributions to the physical broadening of the reflection profiles from the magnitude of the microstrains and the sizes of the coherent scattering regions. To estimate the dislocation density ρ_d , the formula [17,18] was used:

$$\rho_d = 2\sqrt{3} \frac{\langle \varepsilon^2 \rangle^{1/2}}{Db}, \quad (1)$$

where $\langle \varepsilon^2 \rangle^{1/2}$ are root-mean-square microstrains of the B2 phase crystal lattice, D is the size of coherent scattering regions, and b is the Burgers vector of dislocations.

The tensile test specimens were cut on an electric discharge machine in the form of a double blade with a working base of 7 mm. The surface of the samples was polished manually using abrasive paper based on silicon carbide with a gradual decrease in grain size to 1200 and then electropolished in an electrolyte containing acetic and perchloric acid in a ratio of 70:30. Tensile tests were carried out at room temperature on a Walter+Bai AG LFM 125 testing machine with Dioptr software (Walter-Bai AG, Löhningen, Switzerland). The initial strain rate was 10^{-3} s^{-1} . From 4 to 6 samples with identical true strain specified during abc-pressing were tested. The average data about pseudoyield plateau stress, yield stress and ultimate tensile strength obtained from these tensile tests are presented in Section 3.

3. Results

3.1. Microstructure

As noted in the introduction, the evolution of the microstructure of the $\text{Ti}_{49.8}\text{Ni}_{50.2}$ alloy samples was studied in [14] as a function of the abc-strain specified at 573 K. It was found that the refinement of the grain–subgrain microstructure occurs at two structural-scale levels. The first level (denoted in [14] as a macrolevel) is large grains of initial samples with high-angle grain boundaries. The average sizes of these large grains are denoted as D . The second level (denoted in [14] as the microlevel) is the level of the grain–subgrain structure inside large grains. The average sizes of these grains and subgrains are denoted as d . Studies have shown that to study the patterns of grain refinement at the macrolevel as

a result of SPD, it was possible to use the methods of light optical microscopy and scanning electron microscopy, and to study the grain–subgrain structure, methods of transmission electron microscopy were required. Deformation processes at both structural-scale levels occur simultaneously and influence each other.

A typical intragrain microstructure of the initial coarse-grained samples, shown in Figure 1a, has a microband character. The maximum size of fragments in microbands does not exceed 500 nm. In the microdiffraction pattern, Figure 1b, obtained from the central zone of Figure 1a, there are reflections of the rhombohedral martensitic R phase. It follows from Figure 1c that the sizes of structure fragments of the R phase range from ≈ 50 to 400 nm. The bright-field image of the microstructure in Figure 2a demonstrates the presence of coarse grains in the structure of the samples after abc-pressing at 573 K with a true strain of 1.84. Figure 2a clearly shows the boundary of neighboring large grains. In the grain located on the right side of Figure 2a, an extended microband structure is revealed. The microdiffraction pattern obtained from the central region of this grain, Figure 2b, shows the presence of the R phase, the dark-field image of fragments of which is shown in Figure 2c. As the true strain increases to 5.40, 7.43, and 9.55, the microstructures of the samples are qualitatively similar. As an example, Figure 3 shows micrographs of the microstructure of the sample after abc-pressing to $e = 5.4$. Figure 3a,b show images of the surface obtained by optical microscopy and scanning electron microscopy, correspondingly. Large grains with a maximum size of up to 19 μm are detected by these methods. Figure 3c,d show TEM images of this sample in bright and dark fields, respectively. Figure 3c shows a bright-field image of a microstructure with a thin microband structure inside a grain of a larger scale level (macrolevel). The maximum size of fragments in microbands does not exceed 250 nm. It can be seen from Figure 3d that small fragments with the R phase structure are mainly localized along the boundaries of larger fragments.

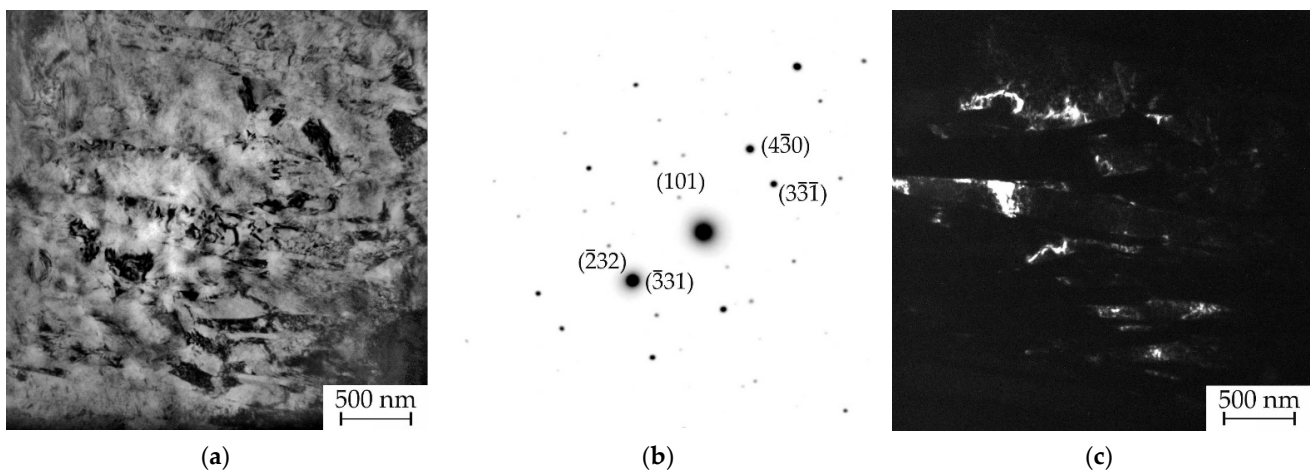


Figure 1. The bright-field microstructure image (TEM) of the initial samples (a); the microdiffraction pattern from the central zone of Figure 1a (b); the dark-field image, $(4\bar{3}0)$ R phase reflection (c).

The dependences of average sizes of large grains, D , and elements of grain–subgrain structure on microlevel, d , on the value of abc-strain are shown in Figure 4. Note that at the macrolevel, the most noticeable decrease in the average grain size D is observed already after of abs-pressing to $e = 1.84$: from 26 μm in initial samples to 17.8 μm in samples after abc-pressing with $e = 1.84$. With a further increase in e , the average grain size decreases more weakly and D equals 12 μm after abc-pressing with $e = 9.55$. According to TEM data, the average size of grains–subgrains d decreases from 350 nm almost linearly with increasing abc-strain and at $e = 9.55$ is 130 nm.

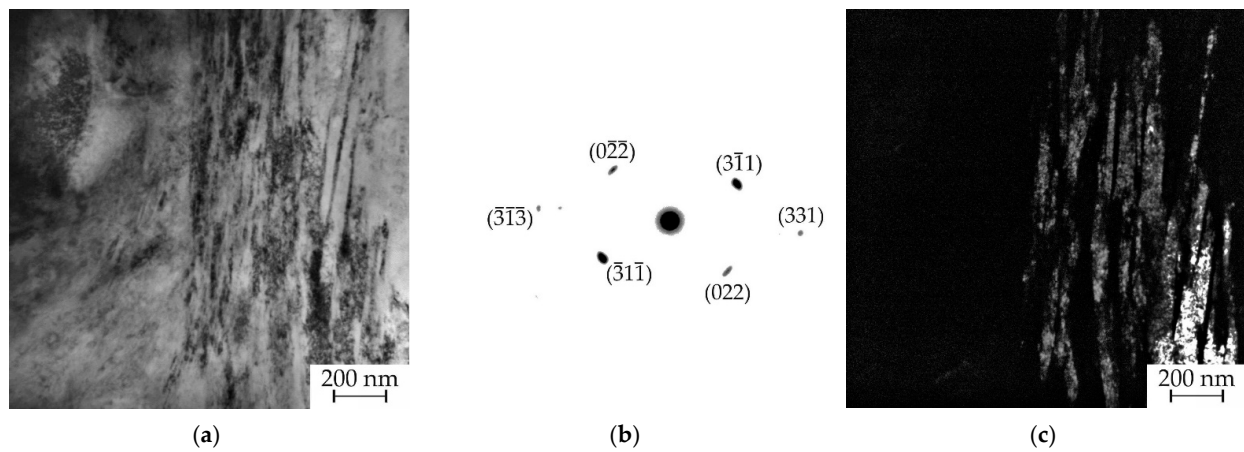


Figure 2. The bright-field microstructure image (TEM) of samples after abc-pressing at 1.84 (a); the microdiffraction pattern from the central zone of right grain (b); the dark-field image, $(\bar{3}1\bar{1})$ R phase reflection (c).

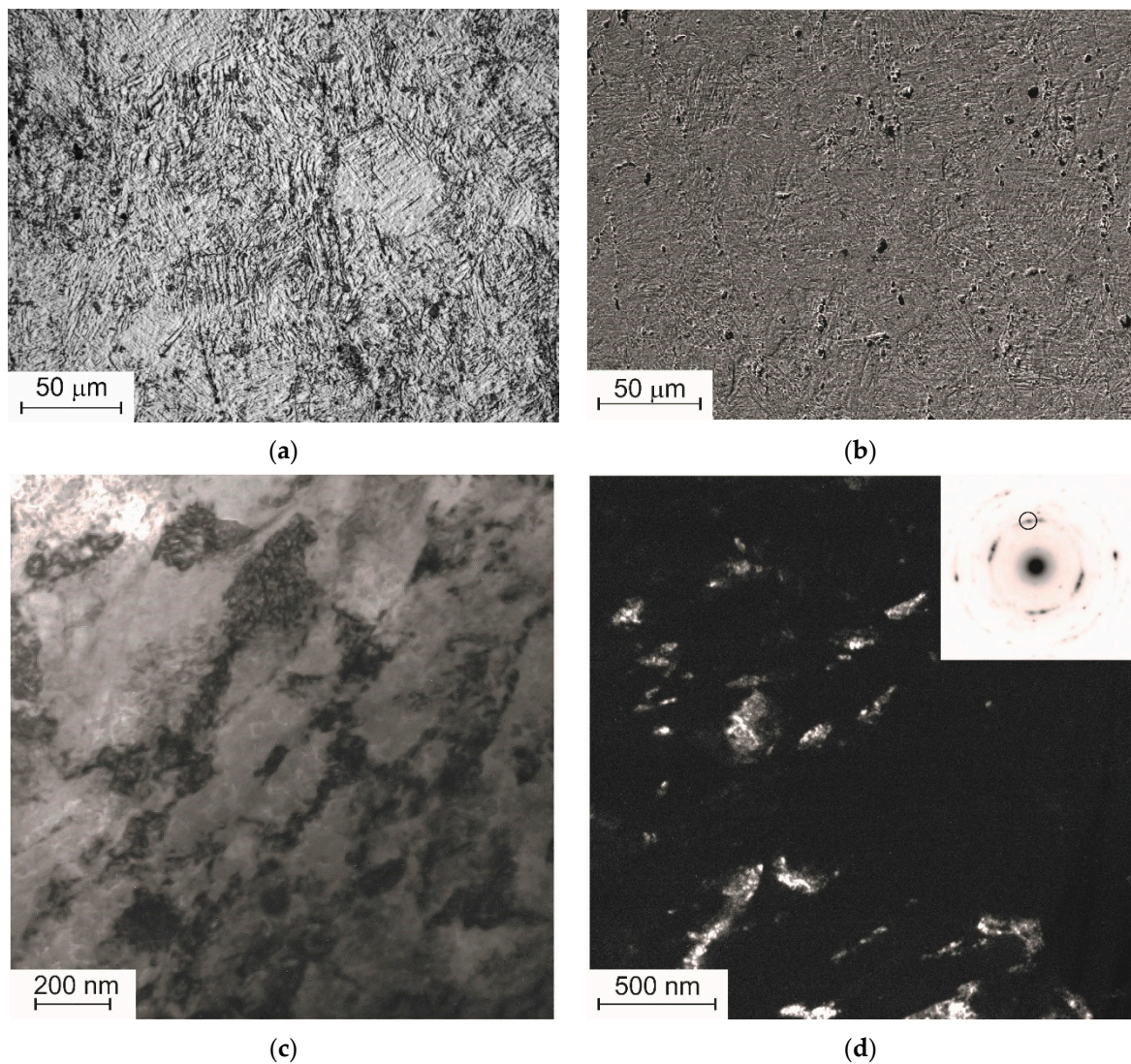


Figure 3. Microstructure of sample after abc-pressing to $e = 5.4$: (a) optical microscopy, (b) scanning electron microscopy, (c,d) transmission electron microscopy (c bright-field image, d dark-field image taken using the R-phase reflection of (211) type which is denoted by circle in insertion).

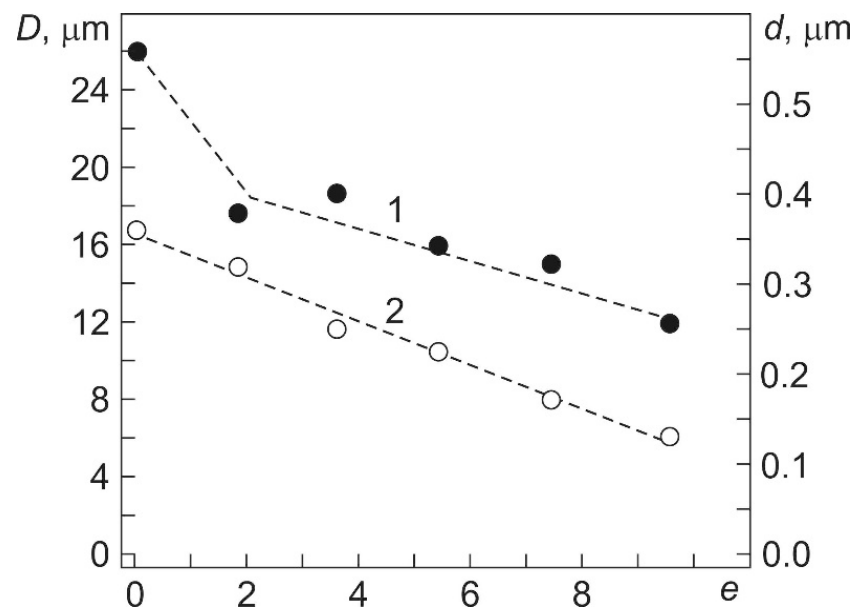


Figure 4. The average size of grains D (curve 1) and grain-subgrains d (curve 2) as the function of abc-strain, e .

Thus, as a result of abc-pressing according to the mode used, with an increase in the abc-strain given to the samples, the elements of the grain-subgrain structure at the microscale level are gradually refined along a linear dependence.

3.2. Mechanical Properties

As noted in Section 2, mechanical tests were carried out at room temperature. According to [14], for all the studied samples, the room temperature is lower than the start temperature of the direct martensitic transformation M_S . Therefore, the main volume of the samples is represented by the R and B19' martensitic phases before the tension test. Figure 5 shows examples of typical engineering tensile diagrams for samples at room temperature for all given values of the true abc-strain. Tensile diagrams are typical for TiNi-based alloys. All diagrams show a quasi-elastic stage (I), a pseudoyield plateau (stage II), a quasi-linear stage of strain hardening (stage III), a parabolic hardening stage (stage IV), and a stage of localized deformation with necking (stage V).

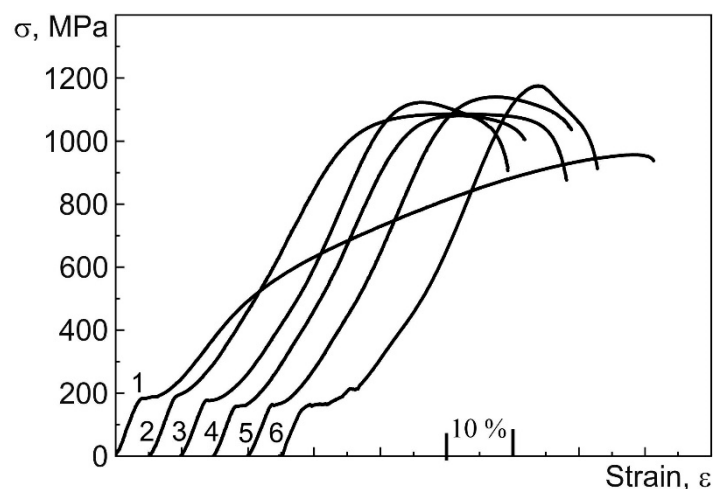


Figure 5. Engineering “stress–strain” curves during tension of titanium nickelide samples in the initial state (1) and after abc-pressing with $e = 1.84$ (2); 3.60 (3), 5.40 (4), 7.43 (5); 9.55 (6).

The stress of the beginning of pseudoyield plateau, σ_m , the yield stress, σ_y , and ultimate tensile strength, σ_{UTS} , versus the true abc-strain, e , are presented in Figure 6.

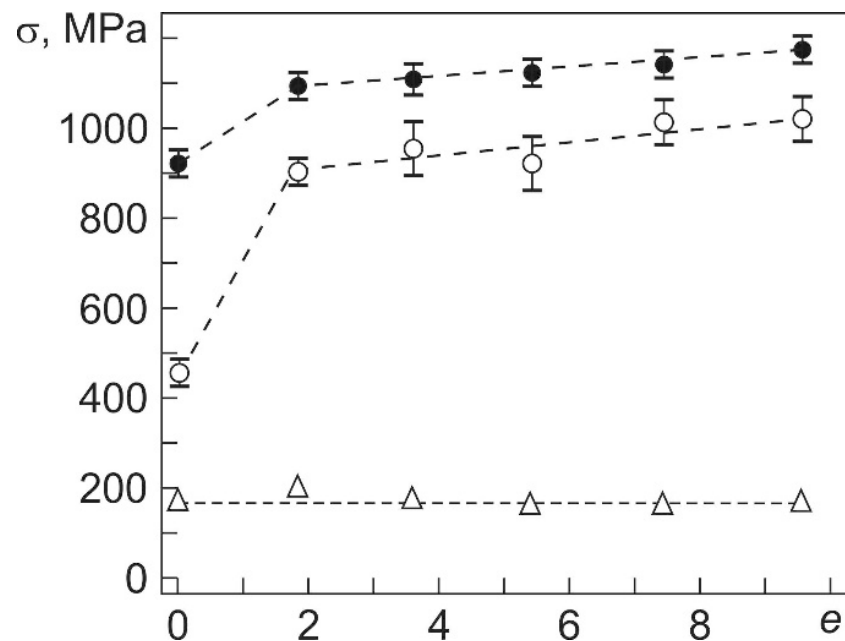


Figure 6. Pseudoyield plateau stress, σ_m (Δ), yield stress, σ_y (\circ), and ultimate tensile strength, σ_{UTS} (\bullet), vs. the true abc-strain, e . Experimental errors of the pseudoyield plateau stress equal ± 20 MPa.

The stress at the beginning of the pseudoyield plateau σ_m for all samples turned out to be almost the same. Since at the test temperature, all the obtained samples are predominantly in the martensitic state, it can be assumed that the deformation of the samples on the pseudoyield plateau is mainly due to the reorientation of the martensitic domains under the action of external stress. Therefore, the refinement of the grain–subgrain structure obtained in the work and the formation of a dislocation substructure during abc-pressing are not effective factors that could affect the stress value of the beginning of the pseudoyield plateau σ_m .

After abc-pressing, even at a true strain $e = 1.84$, the yield stress σ_y turned out to be 900 ± 25 MPa, which is more than twice as high as compared to σ_y in the initial state of the specimens. With a further increase in abc-strain, the yield stress continues to increase rather weakly and reaches 1000 ± 25 MPa at $e = 9.55$ (Figure 6). The ultimate tensile strength σ_{UTS} also increases most noticeably after $e = 1.84$, although this change is much smaller than the change in the yield stress. At the maximum value of the abc-strain given to the samples, their σ_{UTS} increased by about 15%.

The value of the strain-hardening coefficient Θ also changes in a similar way (Figure 7a). An analysis of the $\sigma(\epsilon)$ diagrams showed that the elongation of the samples δ during their tension, both at the ultimate tensile strength and at failure, turned out to be quite high (Figure 7b). Thus, at the value of the maximum abc-strain $e = 9.55$, the uniform elongation of the specimens is about 40%. This figure also shows that already after the first cycle of abc deformation ($e = 1.84$), there is a sharp decrease in δ . With a further increase in e , the weak decrease in δ is observed, as shown in Figure 7b.

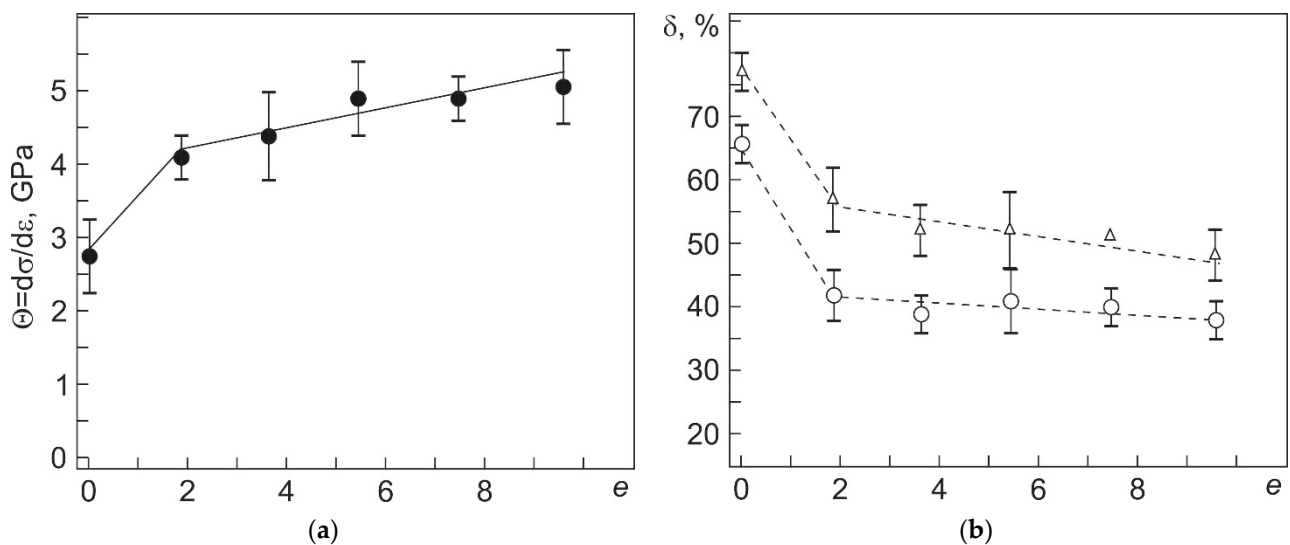


Figure 7. The strain-hardening coefficient (●) at the quasi-linear stage of deformation of the samples (a) and the values of elongation to the ultimate tensile strength, (○), and to the failure of the samples, (Δ), (b) as the function of the true strain.

4. Discussion

Previously, it was shown that after abc-pressing of $\text{Ti}_{49.8}\text{Ni}_{50.2}$ (at %) alloy samples at 723 K [13], the temperatures of martensitic transformations $\text{B2} \rightarrow \text{R}$ and $\text{R} \rightarrow \text{B19}'$ practically do not change, and after abc-pressing at 573 K [14], they change slightly. In this case, the phase composition of the alloys at room temperature remains practically unchanged after pressing at 723 K to 8.44 [13] and at 573 K to 9.55 ([14] and in this work): the B19' martensitic phase with a monoclinic structure, the martensitic rhombohedral R phase, and a small amount of B2 phase. In the process of tension at room temperature of the samples after pressing at 723 K [15] and 573 K (in this work), a pronounced pseudoyield plateau was observed, the beginning of which corresponded to the stress $\sigma_m = 180$ MPa (σ_m is the martensitic shear stress), and σ_m did not change depending on given strain during abc-pressing. This means that the formation of a submicrocrystalline structure with an average grain–subgrain size of ≈ 130 nm in the $\text{Ti}_{49.8}\text{Ni}_{50.2}$ (at %) alloy does not affect the process of reorientation of the initial domains of the martensite phases and the development of the martensitic transformation $\text{R} \rightarrow \text{B19}'$ initiated by external stresses at tensile of samples.

It should be noted that in the initial coarse-grained samples, no difference was found not only in σ_m but also in σ_y (450 MPa) and σ_{UTS} (930 MPa) despite the difference in the average grain sizes in them: 40 μm in [13] and 26 μm in this work. At the same time, after pressing at 723 K with an increase in e to 8.44 in [13], σ_y is systematically less than after abc-pressing at 573 K with an increase in e to 9.55. In particular, σ_y after pressing at 723 K with $e = 8.44$ is 900 MPa in [15], and after pressing at 573 K with $e = 9.55$ $\sigma_y = 1000$ MPa. The tensile strength σ_{UTS} after pressing at 723 K with increasing e up to 8.44 is also systematically lower than after pressing at 573 K with increasing e up to 9.55 (σ_{UTS} is 1000 MPa and 1170 MPa, respectively). In general, this correlates with a more intense refinement of the grain–subgrain structure of the alloy as a result of pressing at 573 K (the average grain–subgrain size reaches 0.13 μm) than after pressing at 773 K in [13] (the average grain–subgrain size is 1 μm).

It follows from the above research results that the main tensile deformation characteristics of the samples of the alloy under study (yield stress and ultimate tensile strength, strain-hardening coefficient, elongation) change most significantly after pressing to $e = 1.84$. With a further increase in the abc-strain, these changes are much less pronounced. Of course, $e = 1.84$ is already a very large strain, which leads to a significant increase in the concentration of defects in the crystal structure (in particular, vacancies and dislocations).

Our measurements of the dislocation density by X-ray diffraction analysis after the strain $\epsilon = 1.84$ specified during abc-pressing at 573 K showed that the dislocation density increases by almost an order of magnitude compared to the initial state ($\approx 1 \times 10^{14} \text{ m}^{-2}$) and reaches $1 \times 10^{15} \text{ m}^{-2}$. The results of the study of defects in the crystal structure formed in samples after pressing with ϵ from 1.84 to 9.55 will be published after their completion. We believe that the density of dislocations is the determining factor in the influence on the value of the yield stress and the coefficient of strain hardening at the quasi-linear stage (III) of the $\sigma(\epsilon)$ dependence. When the samples are deformed at this stage, the deformation is carried out due to the formation of new mobile dislocations. Obviously, the dislocation substructure formed during abc-pressing will prevent the nucleation and motion of these dislocations, which leads to an increase in the yield stress. Thus, it is natural to assume that in samples after abc-pressing at 573 K, the mechanisms of plastic deformation are the same as in coarse-grained samples, despite the fact that as a result of abc-pressing, the average size of the elements of the grain–subgrain structure is effectively reduced to a submicrocrystalline state. The high elongation of the samples to the ultimate tensile strength and fracture testifies in favor of this assumption.

The yield stress of a large group of metals and alloys (including those obtained by SPD methods [2]) depends on the grain size in accordance with the Hall–Petch relation [19,20]:

$$\sigma_y = \sigma_0 + kd^{-1/2}, \quad (2)$$

where σ_0 is a parameter that characterizes the slip resistance of a moving dislocation (friction stress), and k characterizes the ability to transfer deformation from grain to grain and depends on the state of the boundary of neighboring grains. In (2), σ_0 and k are constants. Therefore, the dependence $\sigma_y(d^{-1/2})$ is linear. The experimental dependence $\sigma_y(d^{-1/2})$ after abc-pressing at 573 K of $\text{Ti}_{49.8}\text{Ni}_{50.2}$ (at %) alloy samples is shown in Figure 8. In samples after pressing with ϵ from 1.84 to 9.55, σ_y increases linearly with increasing $d^{-1/2}$. Consequently, similar structures are formed in the strain range from 1.84 to 9.55, for which σ_0 and k are the same. In [21–24], it is believed that the Hall–Petch relation is satisfied not only when the yield stress is reached but also at other strain values (up to the ultimate tensile strength). Figure 8 shows that the dependence of σ_{UTS} on $d^{-1/2}$ is also linear in the strain range ϵ from 1.84 to 9.55. At the same time, the values of σ_y and σ_{UTS} for the original sample are significantly lower than the dependences corresponding to the Hall–Petch relations (Figure 8), which reflects the difference in grain structures and dislocation density in the initial samples and samples after pressing at 573 K. In addition, σ_y and σ_{UTS} can also be affected by other parameters of the microstructure of the samples (for example, the relative fractions of high-angle boundaries of various types), but special studies are needed to confirm this.

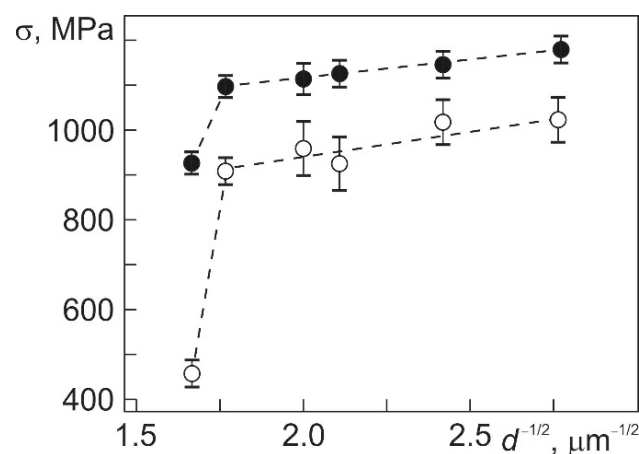


Figure 8. Yield stress, σ_y (○), and σ_{UTS} (●), as a function of $d^{-1/2}$.

The practical importance of obtained $\sigma_y(e)$ dependence may be marked in the final part of the discussion. The abc-pressing at 573 K can be used when it is required to increase the yield stress of material. It is possible to achieve a significant increment in σ_y already after the first pressing cycles with true strains about 2.

5. Conclusions

It has been established that after abc-pressing of $\text{Ti}_{49.8}\text{Ni}_{50.2}$ (at %) alloy samples, already at the value of true strain $e = 1.84$, the yield stress σ_y is equal to 900 ± 25 MPa, which is more than two times higher compared to σ_y in the initial state of samples. With a further increase in the abc-strain, the yield stress of the samples slightly increases and reaches 1000 ± 25 MPa at $e = 9.55$. In this case, the ultimate tensile strength of the samples increases by about 15%. The strain-hardening coefficient $\theta = d\sigma/d\varepsilon$ at the III (linear) stage of the $\sigma(\varepsilon)$ diagrams has a similar dependence on e . It is shown that after abc-pressing from $e = 1.84$ to 9.55 , the yield stress and ultimate tensile strength increase linearly with increasing $d^{-1/2}$ in accordance with the Hall–Petch relation.

It was found that the stress at the beginning of the pseudoyield plateau does not depend on the value of the abc-strain given to the samples. It is supposed that the formation of submicrocrystalline structure in samples of $\text{Ti}_{49.8}\text{Ni}_{50.2}$ alloy during abc-pressing at 573 K does not affect the subsequent reorientation of initial domains of martensitic phases and development of stress-induced $R \rightarrow B19'$ martensitic transformation under tension at room temperature.

Author Contributions: Conceptualization, A.L., V.G. and O.K. (Oleg Kashin); software, K.K.; validation, V.G. and D.Z.; investigations, K.K., D.Z., A.G., N.G., D.B. and O.K. (Olga Kashina); writing—original draft preparation, O.K. (Oleg Kashin) and V.G.; writing—review and editing, V.G. and A.L.; project administration, A.L. and V.G.; funding acquisition, A.L. All authors have read and agreed to the published version of the manuscript.

Funding: This research was funded by Government research assignment for ISPMS SB RAS (project FWRW-2021-0004).

Institutional Review Board Statement: Not applicable.

Informed Consent Statement: Not applicable.

Data Availability Statement: Not applicable.

Conflicts of Interest: The authors declare no conflict of interest.

References

1. Valiev, R.Z.; Zhilyaev, A.P.; Langdon, T. *Bulk Nanostructured Materials: Fundamentals and Applications*; John Wiley & Sons, Inc.: Hoboken, NJ, USA, 2013; p. 440. [[CrossRef](#)]
2. Meyers, M.A.; Mishra, A.; Benson, D.J. Mechanical properties of nanocrystalline materials. *Prog. Mater. Sci.* **2006**, *51*, 427–556. [[CrossRef](#)]
3. Estrin, Y.; Vinogradov, A. Extreme grain refinement by severe plastic deformation: A wealth of challenging science. *Acta Mater.* **2013**, *61*, 782–817. [[CrossRef](#)]
4. Ovid'ko, I.A.; Valiev, R.Z.; Zhu, Y.T. Review on superior strength and enhanced ductility of metallic nanomaterials. *Prog. Mater. Sci.* **2018**, *94*, 462–540. [[CrossRef](#)]
5. Bagherpour, E.; Pardis, N.; Reihanian, M.; Ebrahimi, R. An overview on severe plastic deformation: Research status, techniques classification, microstructure evolution, and applications. *Int. J. Adv. Manuf. Technol.* **2019**, *100*, 1647–1694. [[CrossRef](#)]
6. Kockar, B.; Karaman, I.; Kim, J.I.; Chumlyakov, Y.I.; Sharp, J.; Yu, C.-J.M. Thermomechanical cyclic response of an ultrafine-grained NiTi shape memory alloy. *Acta Mater.* **2008**, *56*, 3630–3646. [[CrossRef](#)]
7. Stolyarov, V.V.; Prokof'ev, E.A.; Valiev, R.Z.; Prokoshkin, S.D.; Dobatkon, S.B.; Trubitsyna, I.B.; Khmelevskaya, I.Y.; Pushin, V.G. Structural Features, Mechanical properties, and the shape-memory effect in TiNi alloys subjected to equal-channel angular pressing. *Phys. Met. Metallogr.* **2005**, *100*, 608–618.
8. Khmelevskaya, I.Y.; Prokoshkin, S.D.; Trubitsyna, I.B.; Belousov, M.N.; Dobatkin, S.V.; Tatyannin, E.V.; Korotitsky, A.V.; Brailovski, V.; Stolyarov, V.V.; Prokofiev, E.A. Structure and properties of Ti-Ni-based alloys after equal-channel angular pressing and high-pressure torsion. *Mater. Sci. Eng. A* **2008**, *481–482*, 119–122. [[CrossRef](#)]

9. Mironov, S.Y.; Salishchev, G.A.; Myshlyaev, M.M.; Pippan, R. Evolution of misorientation distribution during warm 'abc' forging of commercial-purity titanium. *Mater. Sci. Eng. A* **2006**, *418*, 257–267. [[CrossRef](#)]
10. Lotkov, A.I.; Grishkov, V.N.; Dudarev, E.F.; Koval, Y.N.; Girsova, N.V.; Kashin, O.A.; Tabachenko, A.N.; Firstov, G.S.; Timkin, V.N.; Zhapova, D.Y. Ultrafine Structure and Martensitic Transformation in Titanium Nickelide after Warm abc Pressing. *Inorg. Mater. Appl. Res.* **2011**, *2*, 548–555. [[CrossRef](#)]
11. Lotkov, A.I.; Grishkov, V.N.; Kashin, O.A.; Baturin, A.A.; Zhapova, D.Y.; Timkin, V.N. Mechanisms of microstructure evolution in TiNi-based alloys under warm deformation and its effect on martensite transformations. In *Shape Memory Alloys: Properties, Technologies, Opportunities; Materials Science Foundations*; Resnina, N., Rubanic, V., Eds.; Trans Tech Publications Ltd.: Bäch, Switzerland, 2015; Volume 81–82, pp. 245–259. [[CrossRef](#)]
12. Shamsolhodaei, A.; Zarei-Hanzaki, A.; Moghaddam, M. Structural and functional properties of a semi equiatomic NiTi shape memory alloy processed by multi-axial forging. *Mater. Sci. Eng. A* **2017**, *700*, 1–9. [[CrossRef](#)]
13. Kashin, O.; Krukovskii, K.; Lotkov, A.; Grishkov, V. Effect of True Strains in Isothermal abc Pressing on Mechanical Properties of Ti_{49.8}Ni_{50.2} Alloy. *Metals* **2020**, *10*, 1313. [[CrossRef](#)]
14. Kashin, O.; Lotkov, A.I.; Grishkov, V.; Krukovskii, K.; Zhapova, D.; Mironov, Y.; Girsova, N.; Kashina, O.; Barmina, E. Effect of abc Pressing at 573 K on the Microstructure and Martensite Transformation Temperatures in Ti_{49.8}Ni_{50.2} (at%). *Metals* **2021**, *11*, 1145. [[CrossRef](#)]
15. Warren, B.E.; Averbach, B.L. The separation of cold-work distortion and particle size broadening in X-ray patterns. *J. Appl. Phys.* **1952**, *23*, 497. [[CrossRef](#)]
16. Krill, C.E.; Birringer, R. Estimating grain-size distributions in nanocrystalline materials from X-ray diffraction profile analysis. *Philos. Mag. A* **1998**, *77*, 621–640. [[CrossRef](#)]
17. Williamson, G.K.; Smallman, R.E., III. Dislocation densities in some annealed and cold-worked metals from measurements on the X-ray Debye-Scherrer spectrum. *Phil. Mag.* **1956**, *1*, 34–46. [[CrossRef](#)]
18. Smallman, R.E.; Westmacott, K.H. Stacking faults in face-centred cubic metals and alloys. *Phil. Mag.* **1957**, *2*, 669–683. [[CrossRef](#)]
19. Hall, E.O. The deformation and ageing of mild steel: III. Discussion of results. *Proc. Phys. Soc.* **1951**, *64*, 747–753. [[CrossRef](#)]
20. Petch, N.J. The cleavage strength of polycrystals. *J. Iron Steel Inst.* **1953**, *174*, 25–28.
21. Hirth, J.P.; Lothe, J. *Theory of Dislocations*, 2nd ed.; N-Y. J. Wiley & Sons, Inc.: Hoboken, NJ, USA, 1982; p. 857.
22. Gleiter, H. Nanostructured materials: Basic concepts and microstructure. *Acta Mater.* **2000**, *48*, 1–29. [[CrossRef](#)]
23. Kozlov, E.V.; Zhdanov, A.N.; Koneva, N.A. Barrier Retardation of Dislocations. Hall-Petch Problem. *Phys. Mesomech.* **2006**, *9*, 75–86.
24. Armstrong, R.W. Dislocation and grain size roles in physical mesomechanics. *Phys. Mesomech.* **2021**, *24*, 418–425. [[CrossRef](#)]